Competitive Adsorption and Reduced Mobility: N-Octane, CO_2 and H_2S in Alumina and Graphite Pores

Sakiru B. Badmos, Naimul Islam, Urvi Shah and Alberto Striolo*

Department of Chemical Engineering
University College London
London, WC1E 7JE, UK

David R. Cole

School of Earth Sciences
The Ohio State University
Columbus, Ohio 43210, USA

ABSTRACT

Because gas injection into geological formations is a common technology deployed for enhanced oil recovery (EOR), it is important to understand at the molecular level the relations between competitive adsorption and fluid mobility at the single-pore level. To achieve such an understanding, we report here molecular dynamics simulation results to document structural and dynamical properties of *n*-octane confined in slit-shaped alumina and graphite pores in the presence of CO_2 or H_2S. The substrates are chosen as proxy models for natural hydrophilic and hydrophobic substrates, respectively. It was found that CO_2 and H_2S could displace *n*-octane from alumina but not from graphite surfaces. Analysis of the results demonstrates that more attractive *n*-octane – surface and weaker CO_2/H_2S – surface interactions in graphite compared to alumina are responsible for this observation. Regardless of pore type, the results suggest that adding CO_2 or H_2S suppresses the diffusion of *n*-octane due to pore crowding. However, the mechanisms responsible for this observation are different, wherein preferential adsorption sites are available on the alumina surface for both CO_2 and H_2S, but not on graphite. To contribute to designing advanced EOR technologies, possible molecular mechanisms are proposed to interpret the results.

1.0 INTRODUCTION

The quest for sustainable and environmental-friendly energy sources coupled with depletion of global oil reserves has stimulated research into shale gas and oil production. Shale rocks mainly consist of clay, quartz, pyrites, carbonates (inorganic) and kerogen (organic) with many pores in the nanometer-size range.[1-3] Pores found in shale have poor connectivity, resulting in low permeability. To overcome such low permeability, hydrocarbon production from shale plays is achieved via horizontal drilling and hydraulic fracturing, although most of the hydrocarbons remain in place and the production rate drops rapidly.[4] Enhanced oil recovery (EOR) has been proposed for increasing hydrocarbon production from shale formations, and it is also widely practiced in conventional formations globally. When supercritical carbon dioxide (CO_2) is used in EOR, the technology could help achieve CO_2 sequestration in geological formations while contributing to increased hydrocarbon production. It has also been suggested that hydrogen sulphide (H_2S) could be used for similar applications.[5] In our recent study,[6] we employed molecular dynamics (MD) simulations to quantify whether CO_2 and H_2S displace *n*-butane from silica, muscovite and MgO surfaces. It was found that both gases perform reasonably well in silica and muscovite, but poorly in the model MgO substrate. Our study showed that the results depend on competitive adsorption among the confined fluids (hydrocarbons and acid gases) on the substrate. To complement our prior studies, which only considered inorganic substrates, in this manuscript we quantify the ability of CO_2 and H_2S to displace *n*-octane from one model inorganic hydrophilic surface and one hydrophobic substrate. Because the hydrocarbons are more strongly attracted to graphite, CO_2 and H_2S might not be as effective in displacing the hydrocarbons as they are on alumina. It should be noted that graphite has been used extensively as a proxy for mature organic matter present in shales.[7-12]

Several studies have been conducted for CO_2-hydrocarbon systems confined in inorganic[13-21] and carbon nanopores.[7, 12, 22-25] Yuan et al.[23] performed MD simulations to study methane (CH_4) and CO_2 in carbon nanopores and found that CO_2 is more strongly adsorbed on graphite than CH_4, resulting in CO_2 displacing CH_4 from the graphite surface. Building on these results, Yuan et al. found an optimal pore diameter for CH_4 recovery. Liu et al.[7] studied binary CH_4 and CO_2 systems in graphite nanochannels, and found preferential CO_2 adsorption on graphite coupled with a longer residence time. Wu et al.[12]

found that both N_2 and CO_2 could displace adsorbed CH_4 from carbon nanochannels. They reported that while CO_2 replaced the adsorbed CH_4, N_2 enhanced CH_4 displacement by lowering its partial pressure. Sun et al.[15] studied CH_4 and CO_2 confined in silica, calcite and graphite nanopores and found that CH_4 is more strongly adsorbed on graphite compared to silica and calcite, and that CO_2 is more strongly attracted to calcite than silica and graphite. Although most studies focussed on CH_4, a few considered longer alkane molecules on graphite.[26-28] To complement such studies as well as our prior work on confined hydrocarbons and acid gases,[6] in the present study we simulate *n*-octane, CO_2 and H_2S.

In this manuscript, we investigate the displacement of *n*-octane from alumina and graphite surfaces due to the addition of CO_2 and H_2S as well as structural and dynamical properties of the confined fluids. The pores considered are dry and therefore pH effect on the pore surfaces are not considered.

The remainder of this manuscript is organized as follows: in Section 2 we describe the simulation models and algorithms implemented in this study; in Section 3 we present the simulation results; we then conclude by briefly discussing and summarizing our main findings.

2.0 SIMULATION MODELS AND METHODOLOGY

2.1 Simulation set up

Equilibrium molecular dynamics (MD) simulations were conducted for binary mixtures of CO_2/*n*-C_8H_{18} and H_2S/*n*-C_8H_{18} confined within slit-shaped alumina and graphitic pores of width 2.2nm. The pore width is consistent with some of the pores found in shale, which are in the range of 1.7 – 20 nm.[29] The simulations were conducted to investigate the effect of the addition of CO_2 or H_2S on the behaviour of the confined *n*-octane at 350K.

We recently conducted MD simulations to investigate the displacement of *n*-butane from silica, muscovite and MgO surfaces by addition of CO_2 or H_2S.[6] All surfaces considered in the previous study were inorganic, where we found that the effectiveness of the gas at displacing *n*-butane from the surfaces depends on gas – surface interactions. Here, we consider one inorganic pore (alumina) and one carbon-

based pore, modelled as graphite. We seek to understand the interactions of the volatile gases with the surfaces and the implications on the behaviour of the confined *n*-octane.

Alumina slabs are modelled as crystallographic faces of sapphire α-Al_2O_3 with space group R3c and C plane (0001). Two alumina slabs facing each other within the simulation box form the slit shaped pore. The pore width is the centre-to-centre distance between the hydroxyl groups on the two alumina slabs across the pore volume. All the non-bridging oxygen atoms were protonated, yielding a realistic model for the alumina surface.[30] Slit-shaped alumina pores have been used previously to study fluid behaviour in nanopores.[31-35]

Graphite pores were obtained from two 4-layered graphite slabs with interlayer spacing of 0.34 nm facing each other across a pore of with 2.2 nm. The pore width of the graphitic pore is defined as the distance between the planes passing through the outermost graphene layers of the two slabs.

The planar dimensions of the alumina and graphite slabs are 47.6 x 90.68 $Å^2$ and 48.92 x 90.86 $Å^2$, respectively, yielding alumina and graphite pores of approximately equal pore surface area. Each slab of the substrate is parallel to the X-Y plane of the simulation box. The Z-dimension of the simulation box was set to 45.82 and 42.05Å for alumina and graphite, respectively, to achieve a similar pore volume in the two systems.

All atoms within the solid substrates were held fixed, except the –OH groups on alumina, which were allowed to vibrate. Due to the application of periodic boundary conditions, the systems are infinitely long in X and Y directions and the pore width is defined along the Z direction.

Binary systems of *n*-C_8H_{18} – CO_2 and *n*-C_8H_{18} – H_2S were simulated at different gas loadings and constant number of *n*-C_8H_{18} molecules. The compositions of the simulated systems are reported in **Table 1**. **Figure 1** shows representative snapshots for *n*-octane – H_2S and *n*-octane – CO_2 systems for maximum gas loading in alumina and graphite pores. The system pressure changes as the system composition and the number of fluid molecules in the pores change. To estimate the pressures considered in our study, we calculate the average densities of *n*-octane and gas molecules at the middle of the pores and we then use the Peng-Robinson equation of state, as available in the REFPROF

software, version 9.1.[36] The results are reported in **Table 1**. These data should only be considered as tentative guidelines, as it is known that confinement in pores alters the thermodynamic properties of fluids.[37-40] In particular, extended Peng-Robinson equations of state have been used to predict fluid behaviour in cylindrical and slit pores.[41-43]

Table 1: Composition of the systems simulated in this work. In all cases, the simulation temperature was 350K. The pressure in the various systems were estimated from the density in the middle of the pores, which explains the, sometimes, large difference between the pressure estimated in the alumina and that in the carbon pore.

System	Number of *n*-octane	Number of CO_2	Number of H_2S	Estimated Pressure (±0.5 MPa) (Alumina)	Estimated Pressure (±0.5 MPa) (Graphite)
1	200	200	-	6	7.5
2		350	-	39	17.5
3		500	-	177	74
4		-	200	2	3
5		-	350	28	6
6		-	500	120	60
7		-	-	0.02	0.02

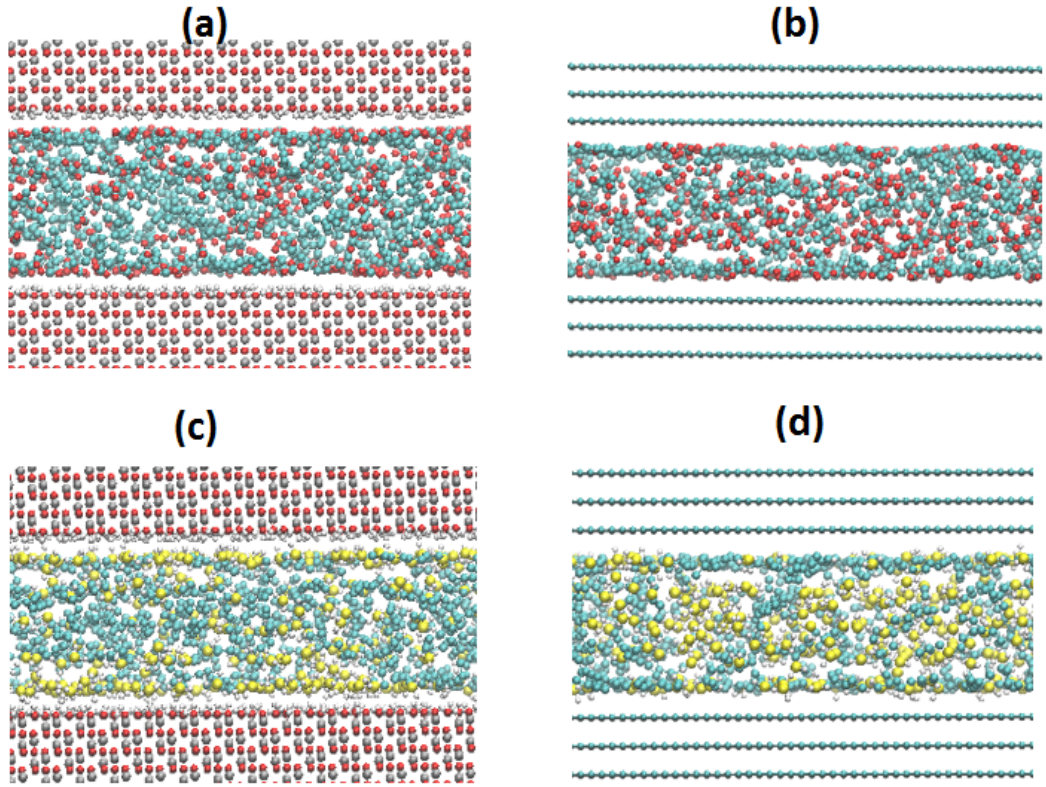

Figure 1: Simulation snapshots for *n*-octane - CO_2 systems in (a) alumina and (b) graphite. Snapshots for *n*-butane - H_2S systems in (c) alumina and (d) graphite. All systems shown contain 200 *n*-octane and 500 gas molecules. Cyan spheres are -CH_3 and -CH_2 in *n*-butane, yellow sulphur, white hydrogen, red oxygen and grey aluminium. For clarity, only a portion of the solid substrates are shown along the Z direction. Please refer to Section 2.1 for details regarding the size of the simulation boxes.

2.2 Force fields

Alumina and graphite were modelled with the CLAYFF[44] force field and the Steele model,[45] respectively. *n*-octane was modelled using the TRAPPE-UA force field,[46] CO_2 with the EPM2 force field,[47] and H_2S with the model developed by Kamath and Potoff.[48] The flexibility of the *n*-octane molecules is enabled by angle bending and dihedral potentials. –CH_3 and –CH_2 groups in *n*-octane were described using the united atom formalism, consistent with the TRAPPE-UA force field.

Non-bonded interactions were modelled by electrostatic and dispersive interactions. The dispersive interactions were described by 12-6 Lennard Jones potential and the electrostatic interactions were modelled by Coulombic potential. There are no electrostatic interactions between CO_2 or H_2S molecules and graphite surface as graphite contains no partial charges in our model. Lorentz-Berthelot

combination rules[49] were used to obtain LJ parameters for unlike atoms. The cut-off distance for all interactions was set to 14Å. The particle mesh Ewald method was used for long range corrections to electrostatic interactions.[50]

2.3 Algorithms

All simulations were performed using the simulation package GROMACS, version 5.0.4,[51-52] in the canonical ensemble (NVT) at 350K. The temperature of the systems was controlled using the Nosé-Hoover thermostat with a relaxation time of 200fs. The temperature of the solid substrate and that of the fluid molecules were controlled separately using two thermostats. The total simulation time for each system was 60 ns. Each system was considered equilibrated when densities of fluid molecules fluctuate around a constant value, and the system energy fluctuates within 10% of the average value. The trajectories from the last 10 ns of the simulations were used for data analysis.

3.0 RESULTS AND DISCUSSION

3.1 Density Profiles

The density profiles of confined fluid molecules in the direction normal to the pore surfaces is used to quantify the distribution of fluid molecules within the pores. The density profiles of the centre of mass (COM) of *n*-octane at different H_2S and CO_2 loadings in alumina and graphite pores are shown in **Figure 2**. The results reveal preferential adsorption of *n*-octane on the pore surfaces, especially when neither CO_2 nor H_2S is present, as shown by high density peaks close to the pore walls compared to the middle of the pore. The adsorption of *n*-octane onto graphite is more pronounced than on alumina, as evidenced by the density of the first adsorption layer in **Figure 2**. This result is consistent with those of Wang et al.,[22] who observed higher peak density for *n*-octane confined in graphite compared to silica pores, signifying strong interaction and preferential adsorption of *n*-octane within graphitic nanopores.

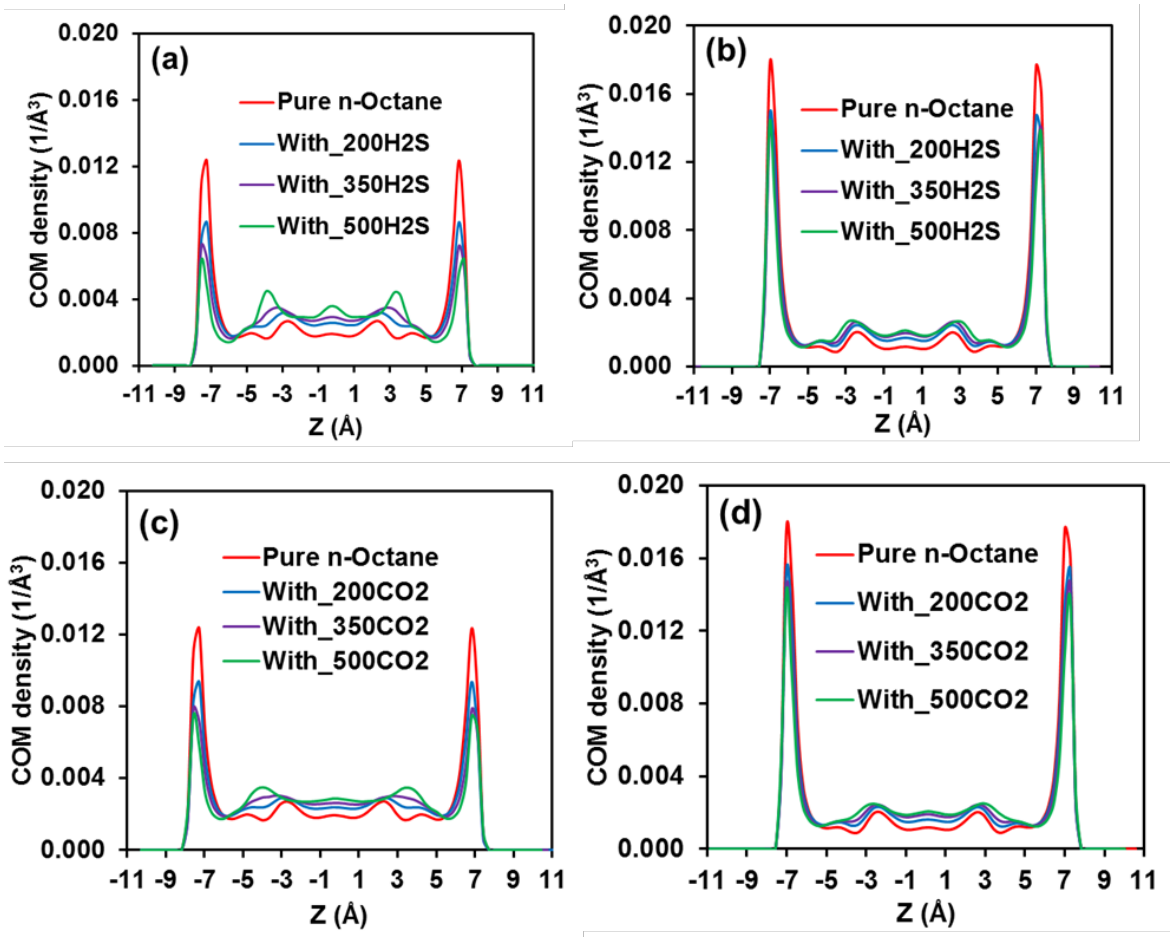

Figure 2: Density profiles of *n*-octane in (a) alumina (b) graphite at different H_2S loadings and density profiles of the centre of mass (COM) of *n*-octane at different CO_2 loadings in (c) alumina and (d) graphite. All systems contain 200 *n*-octane molecules.

The results in **Figure 2** show that adding H_2S or CO_2 to a system containing pure *n*-octane results in the displacement of *n*-octane from alumina surface, as revealed by the decrease in the first peak height. In graphite, however, the reduction in the first peak height only occurs when 200 gas molecules are added, while the first peak remains relatively unchanged with further increases in gas loading. This suggests that CO_2 and H_2S are not effective at displacing *n*-octane from carbon pores, and by extension, pores in mature organic matter as well. The behaviour of *n*-octane in a graphite pore just described is in contrast with the results obtained for *n*-butane in silica, muscovite and MgO pores in our previous study,[6] where the addition of either CO_2 or H_2S resulted in the continuous reduction in the density of *n*-butane molecules in the first adsorbed layer.

The density profiles of H_2S sulphur (S) of H_2S and CO_2 carbon (C) in alumina and graphite pores are shown in **Figure 3**. The density profiles of hydrogen (H) of H_2S and oxygen (O) of CO_2, which complement the results presented in **Figure 3**, are presented in **Figure 4**. These results show that CO_2 and H_2S are more strongly adsorbed on the alumina surface than on the graphite one. This is due to electrostatic interactions between the pore surfaces and the gas molecules, which are possible in alumina but absent in graphite. This stronger interaction between the volatile gases and alumina correlates with their ability at displacing *n*-octane from the pore surface. Although it appears that more H_2S molecules are adsorbed in the first layer in graphite than CO_2, based on the peak features in **Figure 3**, the number of H_2S and CO_2 at comparable loadings, as obtained from the integral of the first density peak, is similar.

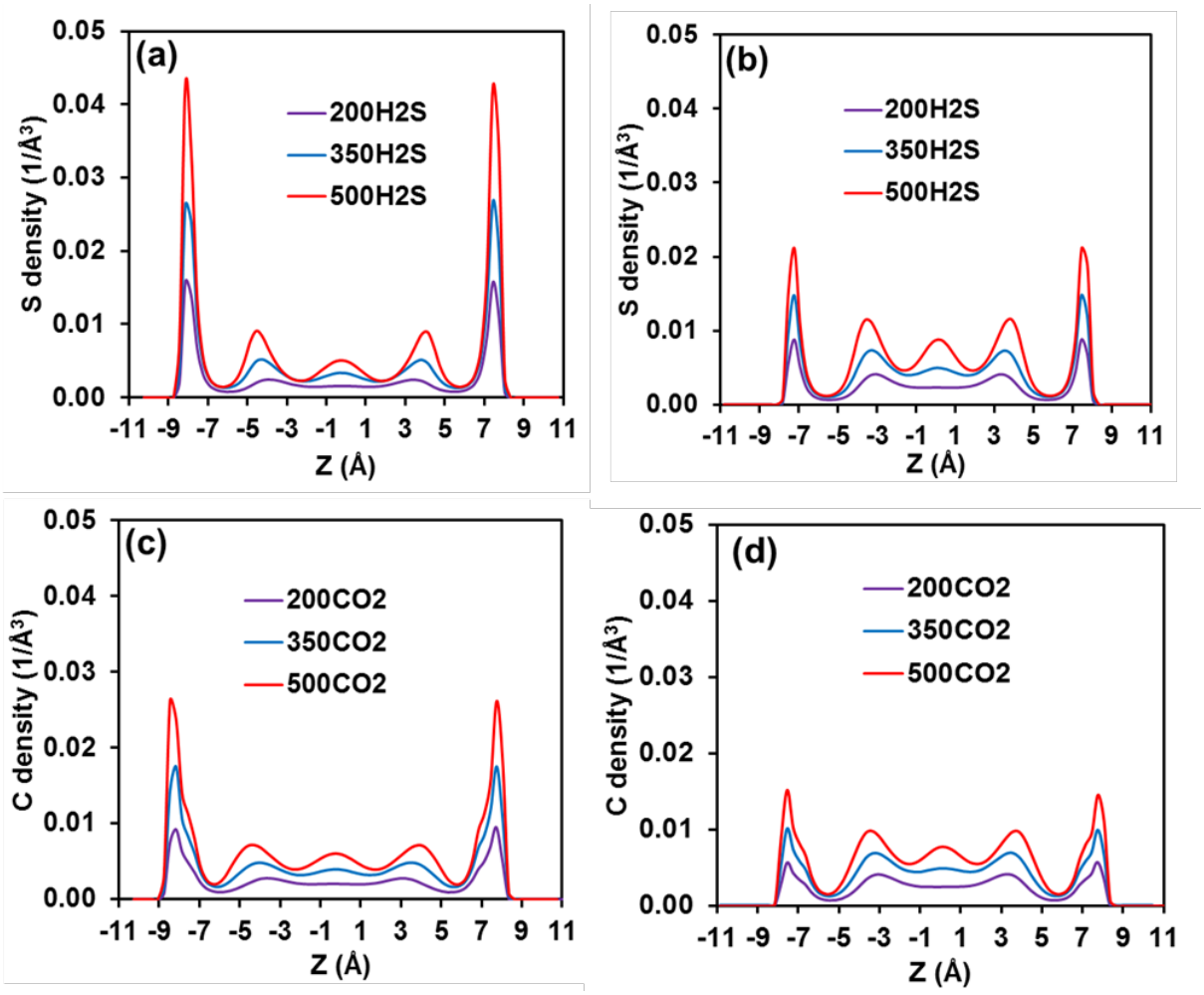

Figure 3: Density profiles of S of H_2S in (a) alumina (b) graphite and density profiles of C of CO_2 in (c) alumina (d) graphite at different acid gas loadings. All systems contain 200 *n*-octane molecules.

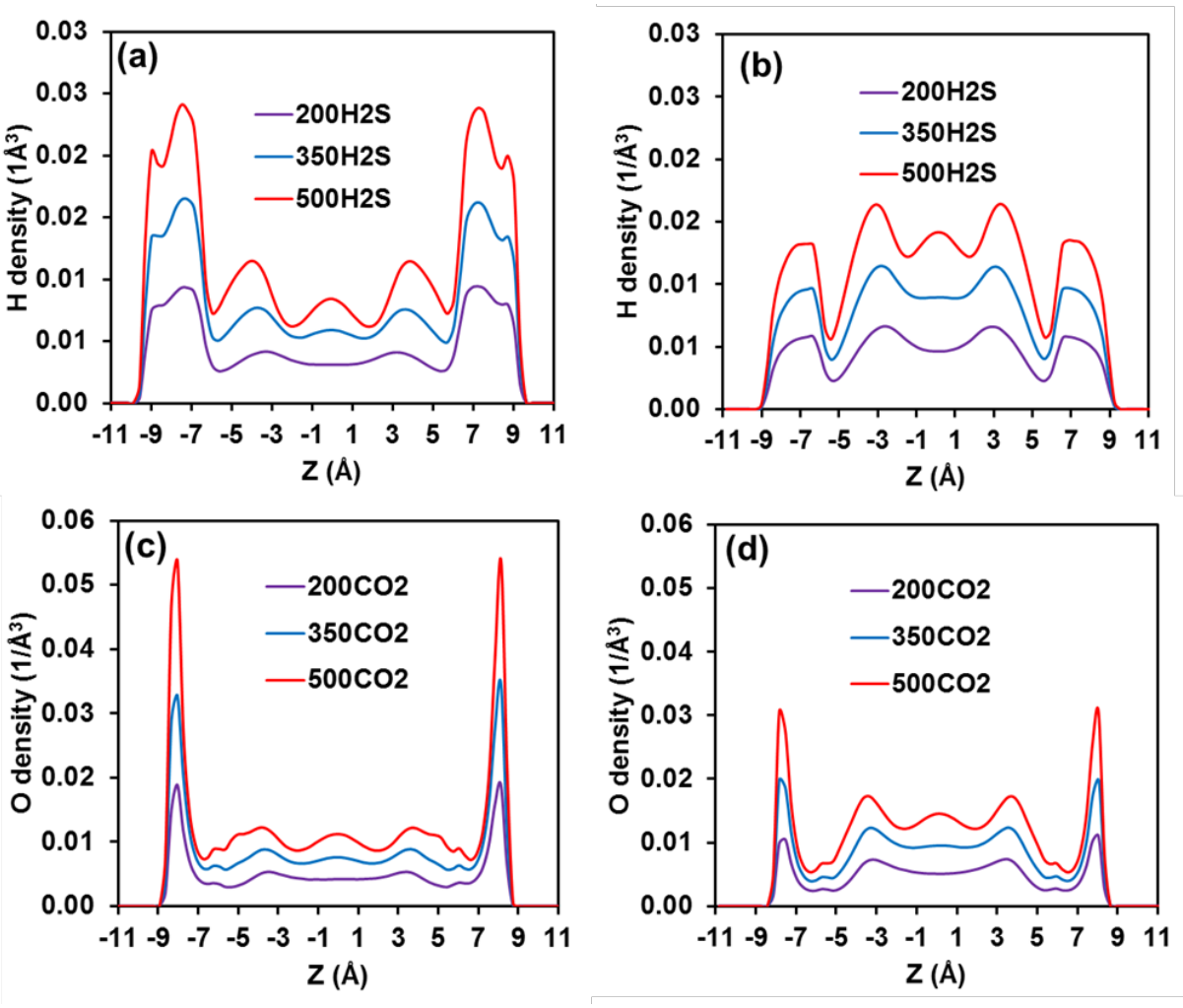

Figure 4: Density profiles of H of H_2S in (a) alumina (b) graphite and density profiles of O of CO_2 in (c) alumina (d) graphite at different acid gas loadings at 350K. All systems contain 200 molecules of n-octane. The simulations are conducted at 350 K.

The results just discussed are obtained on atomically smooth pore surfaces. Surface roughness is likely to affect the competitive adsorption of different fluids, for example because of the resultant uneven distribution of surface –OH groups due to step edges. For example, Le et al.[14, 53] observed higher adsorption of CO_2 near edges on rough silica surfaces, which became effectively more hydrophilic than the surrounding pristine (flat) surfaces due to larger surface density of –OH groups. Therefore, both CO_2 and H_2S could be more effective at displacing hydrocarbons from rough substrates, although this effect is not quantified in the present study.

Another important effect is due to pore width. The amount adsorbed strongly depends on pore size. For example, Chen et al.[54] reported higher adsorption density for CO_2 in narrow than in wider carbon pores. In narrow pores, preferential interactions between the pore surface and selected molecules are more pronounced, although competitive effects due to molecular size and shape become important when the pore width is comparable to the molecular dimensions. Sharma et al.,[55] for example, found higher methane than ethane adsorption on montmorillonite pores due to the molecular structure the fluids assume within the pores. Because various competitive effects strongly depend on pore width, it is expected that varying the pore width will affect the results reported here in non-monotonic ways.

3.2 Interaction energy

In **Figure 5**, we show results for the *n*-octane – surface interaction energy in the binary systems of *n*-octane – H_2S and *n*-octane – CO_2 at different loadings in the two pores considered in this study. The results are normalised per octane molecule. Because *n*-octane does not bear partial charges in our model, the interaction energy shown in Figure 4 is only due to dispersive Lennard-Jones interactions between *n*-octane and the surfaces. The negative sign signifies attraction. The results show that *n*-octane is more strongly attracted to graphite than alumina, as expected. Compared to similar results obtained in other pore types,[6] the results also indicate that *n*-octane interaction energies do not change significantly with gas loading, although they become somewhat less attractive as volatile gases loading increases. The stronger interaction between *n*-octane and graphite surface correlates with the poor ability of both gases to displace *n*-octane from graphite, as shown in the density profiles in **Figure 2** b and d.

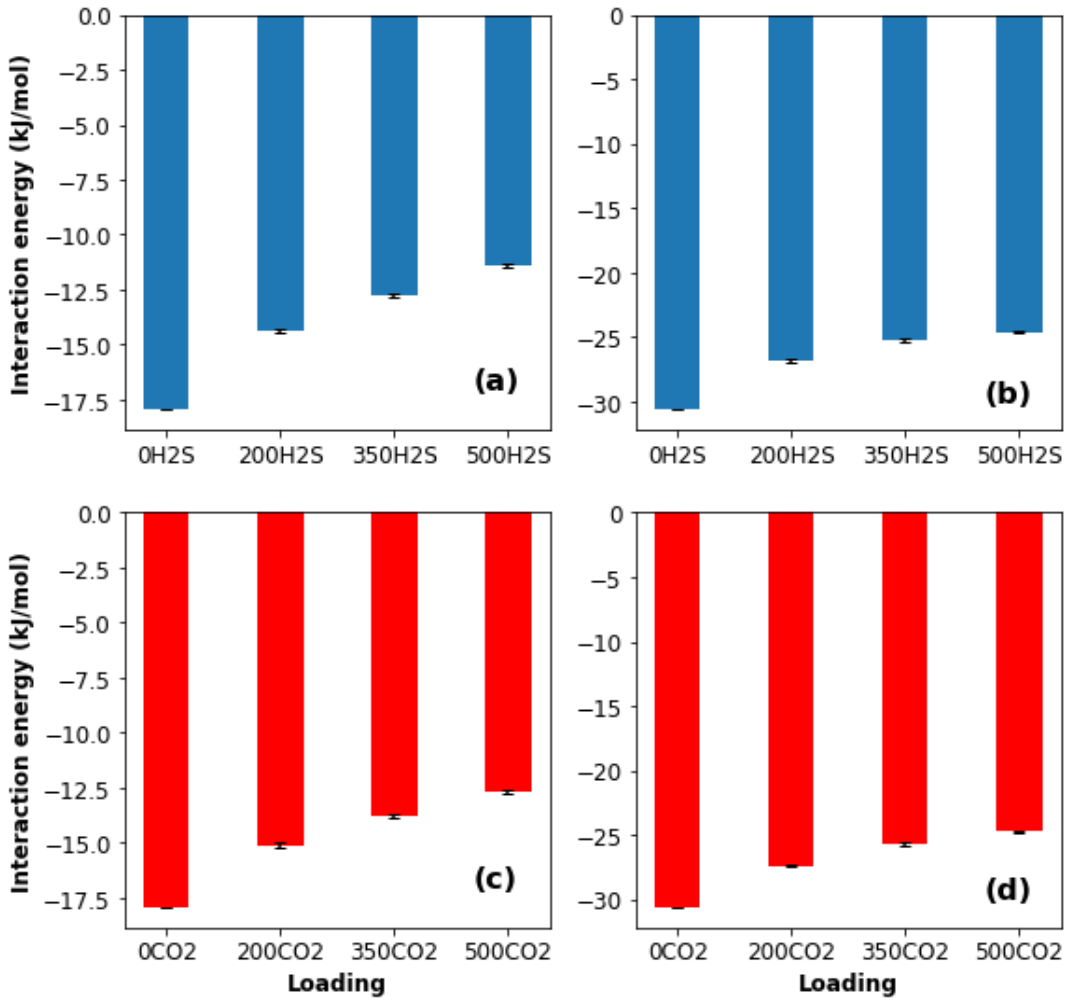

Figure 5: *n*-octane-surface interaction energy for binary systems of *n*-octane – H_2S in (a) alumina (b) graphite and for *n*-octane – CO_2 in (c) alumina (d) graphite. All systems contain 200 *n*-octane molecules. The interaction energies are normalised by the number of *n*-octane in the system. The uncertainties estimated from the standard deviation of block averaging the results during 10 ns of simulations are indicated in the figure.

The complementary data for the CO_2/H_2S – surface interaction energies, normalised per molecule of the volatile gases, are shown in **Figure 6**. In this case, the interaction energy is the sum of Lennard-Jones and electrostatic contributions (except for graphite, which bears no charge). The results show that the volatile gases are more strongly attracted to alumina than graphite. The results also show that the interaction energies do not change significantly with acid gas loading. The more attractive interactions of the acid gases with alumina are consistent with the *n*-octane density profiles in **Figure 2**.

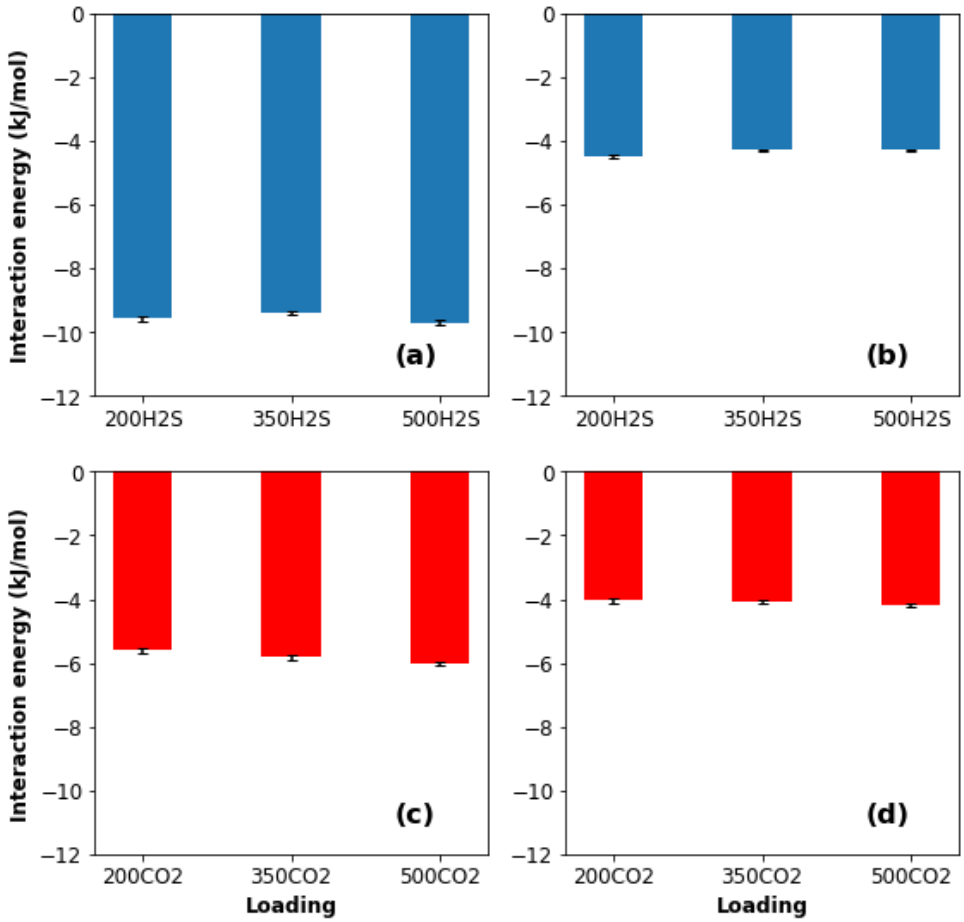

Figure 6: H_2S -Surface interaction energy for binary systems of *n*-octane-H_2S in (a) alumina (b) graphite and CO_2 – Surface interaction energy for binary systems of *n*-octane-CO_2 in (c) alumina (d) graphite. All systems contain 200 *n*-octane molecules at 350K. The interaction energies are normalised by the number of H_2S or CO_2 molecules in the system. The uncertainties estimated from the standard deviation of block averaging the results during 10 ns of simulations are indicated in the figure.

3.3 Structure of adsorbed acid gases

3.3.1 In-plane density distributions

The results discussed above show that CO_2 and H_2S displaced *n*-octane from alumina surface but not from graphite. These observations are consistent with differences in interaction energies. As reported in our previous study,[6] the in-plane density distribution of gas molecules adsorbed on a solid substrate reveals preferential adsorption sites present on the substrate. To quantify these preferential distributions, we plot the in-plane density distribution of CO_2 and H_2S molecules adsorbed on the interfacial layers closest to alumina and graphite. A layer of 2Å was selected for this calculation and the centre of mass

of each molecule was used to identify its position. The results reveal preferential adsorption sites on alumina (**Figure 7**), while on graphite (not shown for brevity) the distribution of the gases is uniform.

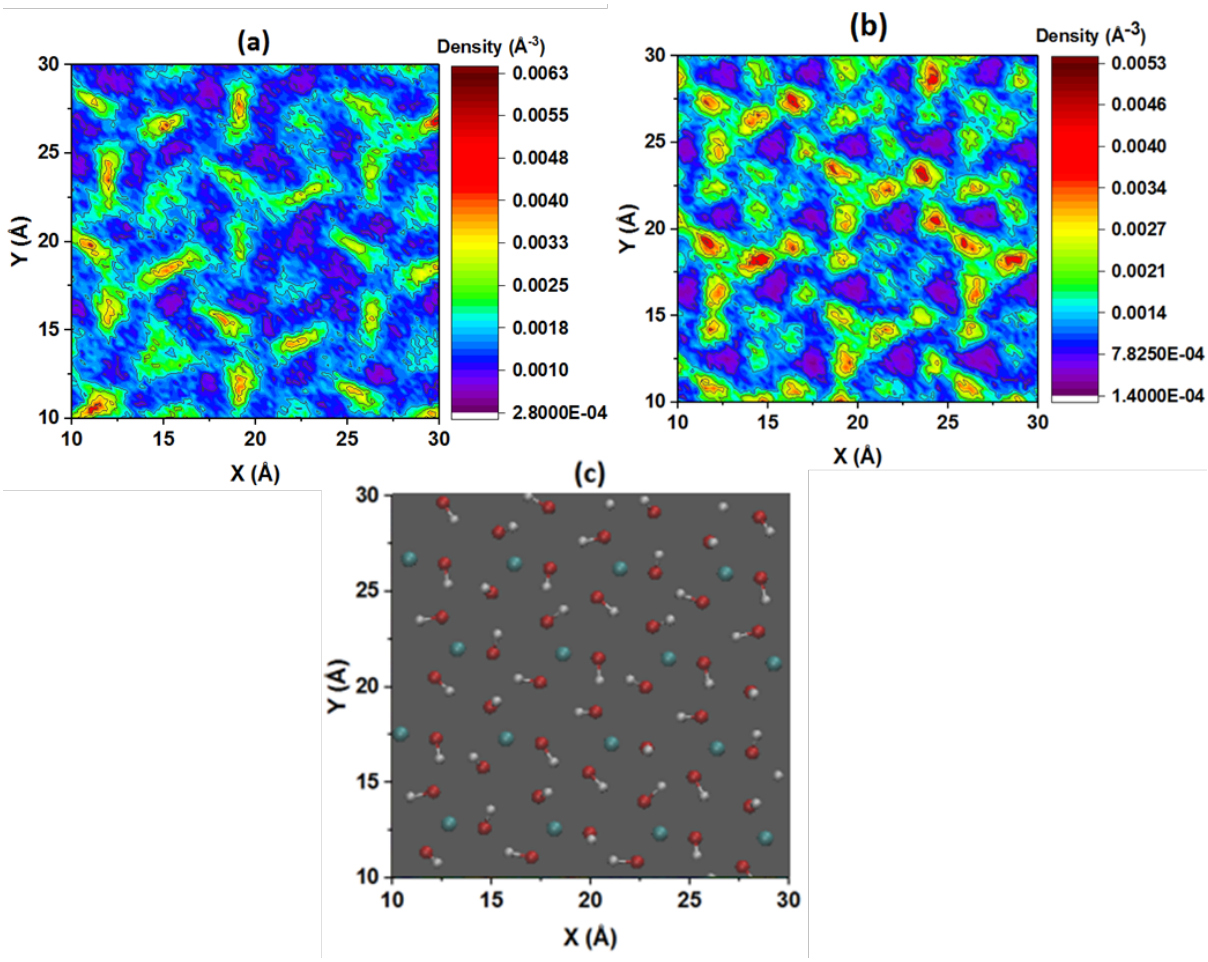

Figure 7: In-plane density distribution of the centre of mass of (a) CO_2 on alumina and (b) H_2S on alumina. All systems contain 200 *n*-octane molecules and 500 molecules of the volatile gas. The simulations are conducted at 350 K. For comparison, in panel (c) the surface structure of the alumina substrate is shown, which helps identify the position of the preferential adsorption sites. In panel (c), red spheres represent oxygen, cyan spheres represent aluminium, and white spheres represent hydrogen. Only the atoms from the solid substrate closest to the pore surface are shown for clarity.

3.3.2 Molecular structure of *n*-octane within the pores

To quantify the structure of *n*-octane molecules adsorbed on the pore surfaces as opposed to that of the molecules near the middle of the pore, we calculate the changes in molecular length as quantified by L, as a function of the position within the pore. L is defined as:

$$L = \frac{l\,(z) - l_0}{l_0} * 100 \qquad (1)$$

In Eq. 1, $l\ (z)$ is the end-to-end distance, expressed in Å, of a single *n*-octane molecule found within a layer located at position z within the simulated pores, and l_0 is the end-to-end distance as a straight chain (8.81Å). Because $l\ (z)$ is always smaller than, or at most equal to l_0, L is expected to be negative. In **Figure 8,** we compare the properties of the *n*-octane molecules found within the first density layer to those of the molecules found within a layer of 8Å centred at the middle of the pore. The results show that *n*-octane molecules in the first adsorbed layer are somewhat shorter on graphite than on alumina, and that some of the *n*-octane molecules adsorbed on both surfaces are more stretched than when they are near the middle of the pore. The latter result is more pronounced on alumina than on graphite surfaces. While qualitatively consistent for both pore types, these results suggest that the chemical nature of the pore surfaces has an influence on the properties of adsorbed *n*-octane.

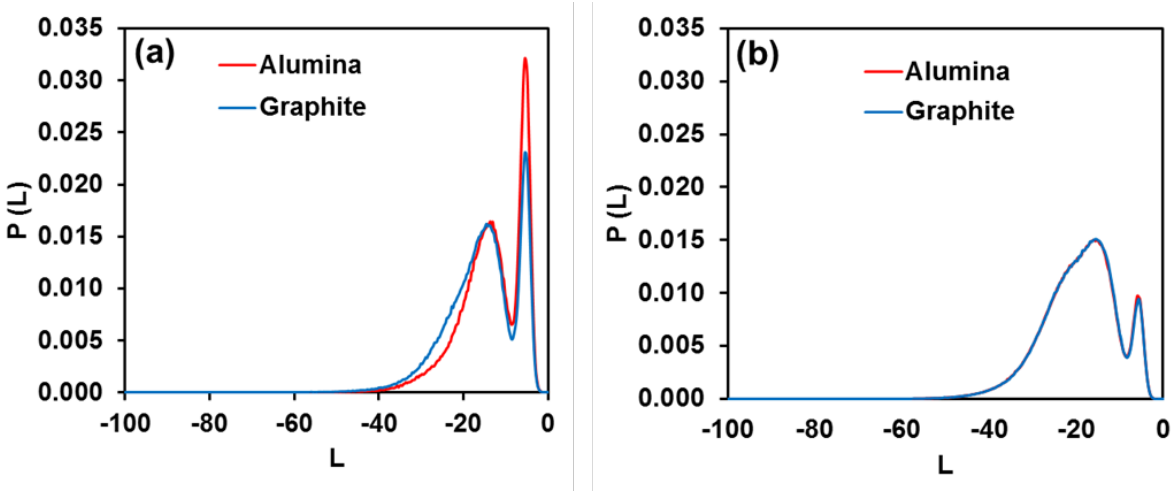

Figure 8: Probability distribution of L for *n*-octane within (a) the first adsorbed layer and (b) the middle region within the slit-shaped pores considered in this work. The results are shown for *n*-octane in graphite and alumina pores in the presence of 500 H_2S molecules. All simulations were conducted at 350 K.

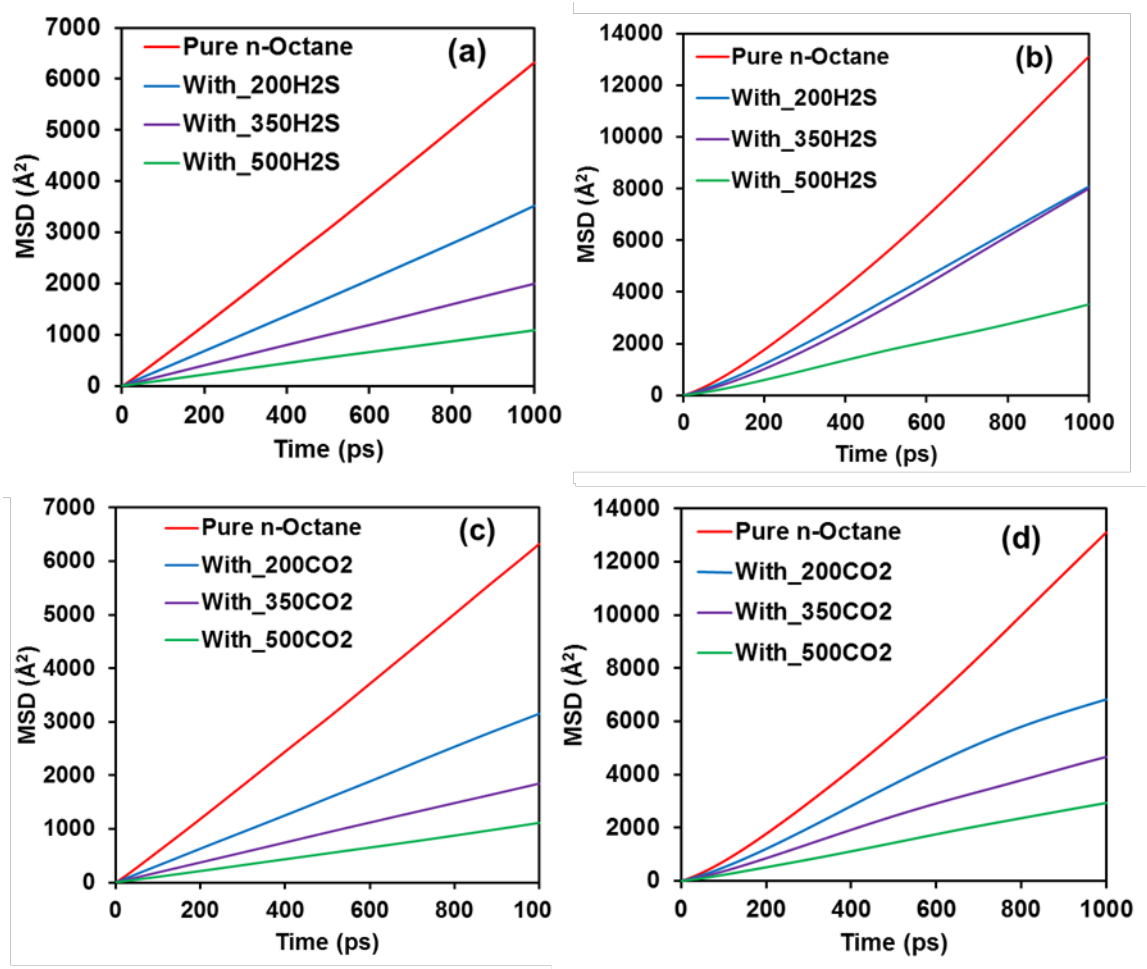

Figure 9: Mean square displacements of the centre of mass of n-octane in systems with increasing amount of H_2S in (a) alumina and (b) graphite pores. Similar results obtained for *n*-octane and CO_2 in (c) alumina and in (d) graphite pores. All simulations are conducted at 350 K.

3.4 Diffusion of confined fluids

The diffusion coefficients of confined fluid molecules were calculated from the mean square displacement (MSD) of the centre of mass of *n*-octane, CO_2 and H_2S, implementing established procedures.[56] The MSD plots are shown in **Figure 9**. It should be noted that simulation box size affects diffusion results estimated from MD simulations[57-59] because of finite-size effects due to the implementation of the periodic boundary conditions.[60] An analytical correction proportional to $N^{-1/3}$ (N being number of molecules in the simulated box) has been proposed to account for such effects. Based on our prior simulations, we expect that the qualitative analysis of the diffusion coefficients as estimated in this study should not be affected significantly by system size effects. The results obtained for fluids confined in graphite and alumina pores are shown in **Table 2** and **3,** respectively, and show that the

diffusion of *n*-octane is slower when CO_2 or H_2S is present in both pores. This suggests that the volatile gases impede *n*-octane diffusion at the conditions of our simulations because of pore-crowding effects. When compared to the estimated diffusion coefficients for liquid n-octane in the bulk as reported by Wang et al.,[61] our results suggest that when confined in the slit-shaped pores considered here, pure n-octane has a faster diffusion in the direction parallel to the pore surfaces. This is probably due to the fact that the density correspondent to the systems with pure octane in our simulations is rather low (see Table 1). In alumina, *n*-octane diffusion coefficient seems to be somewhat greater for *n*-octane – H_2S systems than for *n*-octane – CO_2 systems, especially at lower gas loadings. The diffusion coefficients for CO_2 and H_2S are found to be similar in graphite and alumina pores at comparable loadings, and faster than those obtained for *n*-octane in both pores, as expected given the different molecular size.

Table 2: Self-diffusion coefficients for *n*-octane, CO_2 and H_2S in graphite pores.

System	D (*n*-octane) (10^{-8} m^2/s)	D (CO_2) (10^{-8} m^2/s)	D (H_2S) (10^{-8} m^2/s)
1	1.3 ± 0.2	3.5 ± 0.1	-
2	1.1 ± 0.1	2.4 ± 0.1	-
3	0.7 ± 0.1	1.3 ± 0.1	-
4	2.1 ± 0.2	-	3.4 ± 0.1
5	2.1 ± 0.1	-	2.5 ± 0.1
6	0.9 ± 0.1	-	1.3 ± 0.1
Pure *n*-octane	3.9 ± 0.2	-	-

Table 3: Self-diffusion coefficients for *n*-octane, CO_2 and H_2S in alumina pores.

System	D (*n*-octane) (10^{-9} m^2/s)	D (CO_2) (10^{-8} m^2/s)	D (H_2S) (10^{-8} m^2/s)
1	7.9 ± 0.2	1.4 ± 0.2	-
2	4.6 ± 0.2	0.9 ± 0.1	-
3	2.8 ± 0.1	0.5 ± 0.1	-
4	8.8 ± 0.2	-	1.5 ± 0.1
5	5.0 ± 0.1	-	1.0 ± 0.1
6	2.7 ± 0.1	-	0.5 ± 0.1
Pure *n*-octane	15.9 ± 0.2	-	-

4.0 CONCLUSIONS

Equilibrium MD simulations were conducted to study energetics, structure and transport properties of *n*-octane confined within slit-shaped alumina and graphite pores of width 2.2 nm in the presence of CO_2 or H_2S, at various loadings, at 350K. To complement prior literature results, the present study quantifies the effect of H_2S vs. that of CO_2, taking into account the effect of pore chemistry (inorganic vs. carbon), on the behaviour of confined *n*-octane. The simulated pores are dry but all the non-bridging oxygens on the alumina surface have been protonated. Our results revealed that both H_2S and CO_2 are more efficient at displacing *n*-octane from alumina (inorganic) pore surfaces than from graphite because *n*-octane – surface interactions are much more attractive in carbon than in alumina pores, and because both volatile gases considered are more strongly attracted to alumina than to graphite. Detailed analysis of the simulation results reveals the presence of preferential adsorption sites for H_2S and CO_2 on alumina but not on graphite, which presumably facilitates their ability to displace *n*-octane from the alumina surface. As expected, the structure of *n*-octane adsorbed at the solid – fluid interface is perturbed compared to that in the middle of the pores, as revealed by a notable stretch of the adsorbed molecules, more pronounced on alumina than on graphite. At the simulated conditions, adding CO_2 or H_2S suppresses the mobility of *n*-octane in both pores, which is potentially due to pore crowding. Our results could

contribute to the design of enhanced oil recovery and gas sequestration technologies, which need to be optimised specifically for the properties of the subsurface formations.

ACKNOWLEDGEMENTS

Generous allocations of computing time were provided by the University College London Research Computing Platforms (GRACE&MYRIAD). S.B.B. acknowledges financial support from the Petroleum Technology Development Fund (PTDF). This research received funding from the European Union's Horizon 2020 research and innovation program under Grant No. 764810, within the consortium 'Science4CleanEnergy'. DRC and AS acknowledge research funding received from the U. S. Department of Energy, Office of Basic Energy Sciences, Division of Chemical Sciences, Geosciences and Biosciences under grant DE-SC0006878.

REFERENCES

1. Backeberg, N. R.; Iacoviello, F.; Rittner, M.; Mitchell, T. M.; Jones, A. P.; Day, R.; Wheeler, J.; Shearing, P. R.; Vermeesch, P.; Striolo, A., *Scientific reports* ***7***, 1 (2017).
2. Striolo, A.; Cole, D. R., *Energ. Fuel.* ***31***, 10300 (2017).
3. Ma, L.; Dowey, P. J.; Rutter, E.; Taylor, K. G.; Lee, P. D., *Energy* ***181****, 1285 (*2019**)**.*
4. Sheng, J. J.; Chen, K., *J. Unconv. Oil and Gas Res.* ***5*****,** 1(2014).
5. Khan, C.; Amin, R.; Madden, G., *J. Petrol. Explor. Prod. Technol.* ***3***, 55 (2013).
6. Badmos, S. B.; Bui, T.; Striolo, A.; Cole, D. R., *J. Phys. Chem. C* ***123***, 23907 (2019).
7. Liu, B.; Qi, C.; Mai, T.; Zhang, J.; Zhan, K.; Zhang, Z.; He, J., *J. Nat. Gas Sci. Eng.* ***53***, 329 (2018).
8. Wang, S.; Feng, Q.; Javadpour, F.; Xia, T.; Li, Z., *Int. J. Coal Geol.* ***147***, 9 (2015).
9. Mosher, K.; He, J.; Liu, Y.; Rupp, E.; Wilcox, J., *Int. J. Coal Geol.* ***109***, 36 (2013).
10. Harrison, A.; Cracknell, R.; Krueger-Venus, J.; Sarkisov, L., *Adsorption* ***20***, 427 (2014).
11. Lin, K.; Yuan, Q.; Zhao, Y.-P., *Comp. Mater. Sci.* ***133***, 99 (2017).
12. Wu, H.; Chen, J.; Liu, H., *J. Phys. Chem. C* ***119***, 13652 (2015).
13. Le, T.; Striolo, A.; Cole, D. R., *J. Phys. Chem. C* ***119***, 15274 (2015).
14. Le, T.; Ogbe, S.; Striolo, A.; Cole, D. R., *Mol. Simul.* ***42***, 745 (2016).
15. Sun, H.; Zhao, H.; Qi, N.; Li, Y., *ACS Omega* ***2***, 7600 (2017).
16. Zhang, H.; Cao, D., *Chem. Eng. Sci.* ***156***, 121 (2016).
17. Sun, H.; Zhao, H.; Qi, N.; Qi, X.; Zhang, K.; Li, Y., *Mol. Simul.* ***43***, 1004 (2017).
18. Santos, M. S.; Franco, L. F.; Castier, M.; Economou, I. G., *Energ. Fuel.* ***32***, 1934 (2018).
19. Wang, R.; Peng, F.; Song, K.; Feng, G.; Guo, Z., *Fluid Phase Equilibr.* ***467***, 25 (2018).
20. Pu, J.; Qin, X.; Gou, F.; Fang, W.; Peng, F.; Wang, R.; Guo, Z., *Energies* ***11***, 3045 (2018).

21. Berghe, G.; Kline, S.; Burket, S.; Bivens, L.; Johnson, D.; Singh, R., *J. Mol. Model.* ***25***, 293 (2019).
22. Wang, S.; Javadpour, F.; Feng, Q., *Fuel* ***181***, 741 (2016).
23. Yuan, Q.; Zhu, X.; Lin, K.; Zhao, Y.P., *Phys. Chem. Chem. Phys.* ***17***, 31887 (2015).
24. Furmaniak, S.; Terzyk, A. P.; Gauden, P. A.; Kowalczyk, P.; Harris, P. J., *J. Phys. Condens. Matter* ***26***, 485006 (2014).
25. Lu, X.; Jin, D.; Wei, S.; Zhang, M.; Zhu, Q.; Shi, X.; Deng, Z.; Guo, W.; Shen, W., *Nanoscale* ***7***, 1002 (2015).
26. Sen, W.; Qihong, F.; Ming, Z.; Shuangfang, L.; Yong, Q.; Tian, X.; ZHANG, C., *Petrol. Explor. Dev.* ***42***, 844 (2015).
27. Sammalkorpi, M.; Panagiotopoulos, A. Z.; Haataja, M., *J. Phys. Chem. B* ***112***, 2915 (2008).
28. Park, J. H.; Aluru, N. R., *Chem. Phys. Lett.* ***447***, 310 (2007).
29. Cao, T.; Song, Z.; Wang, S.; Cao, X.; Li, Y.; Xia, J., *Mar. Pet. Geol.* ***61***, 140 (2015).
30. Coustet, V.; Jupille, J., *Surf. Sci.* ***307***, 1161 (1994).
31. Phan, A.; Cole, D. R.; Striolo, A., *Langmuir* ***30*****,** 8066 (2014).
32. Campos-Villalobos, G.; Siperstein, F. R.; D'Agostino, C.; Patti, A *arXiv preprint arXiv:1905.05159 (*2019**).**
33. Phan, A.; Cole, D. R.; Striolo, A., *Langmuir* ***30***, 8066 (2014).
34. De Boer, J.; Lippens, B., *J. Catal.* ***3***, 38 (1964).
35. Pierre, A. C., Springer Science & Business Media, Vol. 1.(2013).
36. Lemmon, E.; Huber, M.; McLinden, M., *Nat. Inst. Stan. Technol.: Gaithersburg (*2013**)**.
37. Srivastava, D.; Santiso, E. E.; Gubbins, K. E., *Langmuir* ***33***, 11231 (2017).
38. Domin, K.; Chan, K.-Y.; Yung, H.; Gubbins, K. E.; Jarek, M.; Sterczynska, A.; Sliwinska-Bartkowiak, M., *J. Chem. Eng. Data* ***61***, 4252 (2016).
39. Gubbins, K. E.; Long, Y.; Śliwinska-Bartkowiak, M., *J. Chem. Thermodyn.* ***74***, 169 (2014).
40. Striolo, A.; Gubbins, K.; Gruszkiewicz, M. S.; Cole, D. R.; Simonson, J. M.; Chialvo, A. A.; Cummings, P. T.; Burchell, T. D.; More, K. L., *Langmuir* ***21***, 9457 (2005).
41. Barbosa, G. D.; Travalloni, L.; Castier, M.; Tavares, F. W., *Fluid Phase Equilibr.* ***493***, 67 (2019).
42. Dong, X.; Liu, H.; Hou, J.; Wu, K.; Chen, Z., *Ind. Eng. Chem. Res.* ***55***, 798 (2016).
43. Islam, A. W.; Patzek, T. W.; Sun, A. Y., *J. Nat. Gas Sci. Eng.* ***25***, 134 (2015).
44. Cygan, R. T.; Liang, J.-J.; Kalinichev, A. G., *J. Phys. Chem. B* ***108***, 1255 (2004).
45. Steele, W. A., *Surf. Sci.* ***36***, 317 (1973).
46. Martin, M. G.; Siepmann, J. I., *J. Phys. Chem. B* ***102***, 2569 (1998).
47. Harris, J. G.; Yung, K. H., *J. Phys. Chem.* ***99***, 12021 (1995).
48. Kamath, G.; Potoff, J. J., *Fluid Phase Equilibr.* ***246***, 71 (2006).
49. Allen, M. P.; Tildesley, D. J., Oxford University Press: Oxford, UK (2004).
50. Essmann, U.; Perera, L.; Berkowitz, M. L.; Darden, T.; Lee, H.; Pedersen, L. G., *J. Chem. Phys.* ***103***, 8577 (1995).
51. Van Der Spoel, D.; Lindahl, E.; Hess, B.; Groenhof, G.; Mark, A. E.; Berendsen, H. J. C., *J. Comput. Chem.* ***26***, 1701 (2005).
52. Abraham, M. J.; Murtola, T.; Schulz, R.; Páll, S.; Smith, J. C.; Hess, B.; Lindahl, E., *SoftwareX* ***1***, 19 (2015).
53. Le, T.; Striolo, A.; Turner, C.H.; Cole, D. R., *Scientific reports* **7**, 1 (2017).
54. Chen, L.; Watanabe, T.; Kanoh, H.; Hata, K.; Ohba, T., *Adsorpt Sci. Technol.* ***36***, 625 (2018)
55. Sharma, A.; Namsani, S.; Singh, J. K., *Mol. Simul.* ***41***, 414 (2015).
56. Kinaci, A.; Haskins, J. B.; Çağın, T., *J. Chem. Phys.* ***137***, 014106 (2012).

57. Le, T. T. B.; Striolo, A.; Cole, D. R., *Mol. Simul.* ***44***, 826 (2018).
58. Yeh, I.-C.; Hummer, G., *J. Phys. Chem. B* ***108***, 15873 (2004).
59. Dünweg, B.; Kremer, K., *J. Chem. Phys.* ***99***, 6983 (1993).
60. Simonnin, P.; Noetinger, B. t.; Nieto-Draghi, C.; Marry, V.; Rotenberg, B., *J. Chem theory comput.* ***13***, 2881 (2017).
61. Wang, S.; Javadpour, F.; Feng, Q., *Fuel* ***171***, 74 (2016).